Formability of Ultrafine-Grained Interstitial-Free Steels

ONUR SARAY, GENCAGA PURCEK, IBRAHIM KARAMAN, and HANS J. MAIER

The stretch formability of ultrafine-grained (UFG) interstitial-free steel (IF-steel) produced by equal-channel angular extrusion/pressing (ECAE/P) *via* various strain paths was investigated with a miniaturized Erichsen test. A coarse-grained (CG) sample demonstrated high formability with an Erichsen index (EI) of 4.5 mm. Grain refinement by ECAE decreased the formability, but increased the required punch load (F_{EI}) depending on the applied strain paths. The EI values were 0.35, 2.90, and 3.91 mm for 8A-, 8Bc-, and 8C-processed samples, respectively. Decrease in the biaxial stretch formability was attributed to the limited strain-hardening capacity of the UFG microstructure. Also, the grain morphology of the UFG microstructure was found to be very influential on stretch formability. Heavily elongated grain morphology in the 8A-processed microstructure resulted in the lowest formability due to the increased cracking tendency through elongated grain boundaries. However, the UFG microstructures with equiaxed grains obtained after 8C and 8Bc ECAE resulted in better formability compared to 8A. The UFG microstructure reduced the roughness (orange peel effect) of the free surface of the biaxial stretched samples by decreasing the non-uniform grain flow leading to the so-called orange peel effect. It should be noted that the strength and ductility values gained from uniaxial tensile tests are not comparable directly to the EI and F_{EI} values determined from the Erichsen tests. Finally, it is important to emphasize that the UFG microstructure produced by a suitable strain path leading to equiaxed grains below 1 μm could be highly deformed even under multiaxial stress conditions.

I. INTRODUCTION

THE fast-growing micro-technology applications require the implementation of smaller products utilizing punching and forming technology. Therefore, miniaturization of parts and plastic-forming applications are gaining attention for applications on a small scale.[1] The coarse grain sizes of the materials to be used in scaled down plastic deformation applications yield a series of problems due to the *size effects* including loss of ductility and strength, higher frictional forces, variability in product dimensions, and free surface roughening.[2] Ultrafine-grained (UFG) materials produced by severe plastic deformation (SPD) with grain sizes in the range of 100 to 1000 nm have received considerable attention due to their higher strength combined with an adequate ductility compared to their coarse-grained (CG) counterparts.[3–13] Among the available SPD methods, equal-channel angular extrusion (ECAE) is considered to be the most capable one to control the resulting

microstructural features of the UFG materials like grain size, grain morphology, and grain boundary character.[14,15] UFG materials have been identified as promising candidates for micro-forming processes due to their submicron-sized structures.[1,2] However, there is lack of knowledge regarding post-SPD processing of shaping of UFG metals, which limits the practical application of UFG metals. A limited number of studies have addressed the promising performance of UFG materials for micro-forming applications. UFG aluminum demonstrated more uniform flow during micro-extrusion[16] and lower surface roughness after micro-bulge tests.[17] Furthermore, UFG copper produced by ECAE yielded a higher punch load and slightly lower limiting drawing ratio.[18] Also, the notable decrease in tensile ductility with increase in strength after ECAE was less pronounced for biaxial ductility.[18]

Interstitial-free steels (IF-steels) contain very low amounts of interstitials like C, N, and O in their ferritic microstructure.[19] The decreased interstitial content results in excellent formability and high normal anisotropy, which provide benefits for sheet metal forming.[20,21] However, the low strength of conventional IF-steels due to the lack of interstitials is a drawback for many applications. Given their mono-phase ferritic microstructure, useful strengthening methods are grain refinement *via* plastic deformation and solid solution strengthening. So far, the tensile response under uniaxial loading and the fatigue behavior of ECAE-processed UFG IF-steel have been investigated systematically,[22–29] and superior strength with acceptable uniaxial tensile

ONUR SARAY, Student, and GENCAGA PURCEK, Professor, are with the Department of Mechanical Engineering, Karadeniz Technical University, 61080 Trabzon, Turkey. Contact e-mail: purcek@ktu.edu.tr, purcek@hotmail.com IBRAHIM KARAMAN, Professor, is with the Department of Materials Science and Engineering, Texas A&M University, College Station, TX. HANS J. MAIER, Professor formerly with the Institut für Werkstoffkunde, University of Paderborn, 33095 Paderborn, Germany, is now with the Institut für Werkstoffkunde, Leibniz Universität Hannover, 30823 Garbsen, Germany.
Manuscript submitted August 2, 2012.
Article published online May 11, 2013

ductility and better low-cycle fatigue performance compared to the CG counterparts have been reported.[23,25,26,30–32] However, the formability behavior, *e.g.*, stretch formability, bendability, and deep drawability, which are the key performance metrics for the applications of the IF-steels, have not been investigated in sufficient detail. Only one study addressed the formability of the IF-steel[33] where accumulative roll bonding (ARB) of the IF-steel resulted in a decrease in the Erichsen value. Processing routes including various strain paths are expected to have a significant effect on the formability of UFG materials,[34] as they affect grain size, grain morphology, and grain boundary characteristics, which in turn control the mechanical properties. To the best of the authors' knowledge, the influence of these factors on the formability has, however, not been investigated in detail.

In view of the above, the purpose of this study was to investigate the stretch formability of UFG IF-steels produced by multi-pass ECAE processing with different microstructural characteristics. Especially, the effect of UFG microstructures with different grain size and grain morphology, obtained by following different strain paths during ECAE processing, on the formability was investigated using a miniaturized Erichsen test. The main objective was to reveal the effect of the SPD-induced UFG microstructure on the biaxial formability of the samples. Given the dimensions of the ECAE billets, the results have most relevance for small-scale applications. As many groups currently work on an upscaling of the established SPD methods, the current results should be applicable for UFG bulk or sheet materials provided that similar microstructures can be established.

II. EXPERIMENTAL PROCEDURE

Ti-stabilized IF-steel, from ERDEMIR Iron–Steel Company-Turkey, with the chemical composition of 0.004 wt pct C, 0.012 wt pct Si, 0.2 wt pct Mn, 0.012 wt pct P, 0.009 wt pct S, 0.1 wt pct Ti, and balance Fe with a mean grain size of about 30 ± 10 μm was used in the present study. For ECAE processing, the billets with the dimensions of 25 mm $\times$ 25 mm $\times$ 150 mm were machined from the hot-rolled plates, such that the longitudinal direction (LD) of each billet coincided with the initial rolling direction. The billets were processed using an ECAE die system with a sharp 90-deg channel cross-sectional angle up to 8 passes following three main ECAE routes: route-A (no rotation of the billet between consecutive passes), route-Bc (the billet was rotated 90 deg counterclockwise around its longitudinal axis between successive passes), and route-C (the billet was rotated 180 deg in the same direction between each pass). The billets covered with a graphite-based lubricant were extruded *via* ECAE at room temperature at a rate of 2.5 mm s^{-1}.

Optical microscopy (OM) and transmission electron microscopy (TEM) were utilized to observe the microstructure of CG and UFG steels, respectively. The samples for optical examination were prepared using standard polishing techniques and then etched with Marshall's reagent. For TEM investigation, 0.5-mm-thick disks were sectioned from the transverse planes (perpendicular to the extrusion direction (ED)) of the extruded billets (Figure 1(a)) and then mechanically ground and polished down to 0.15-mm-thick foils. Large electron-transparent areas were obtained in these foils by conventional twin jet polishing utilizing a 5 pct perchloric acid solution under an applied potential of
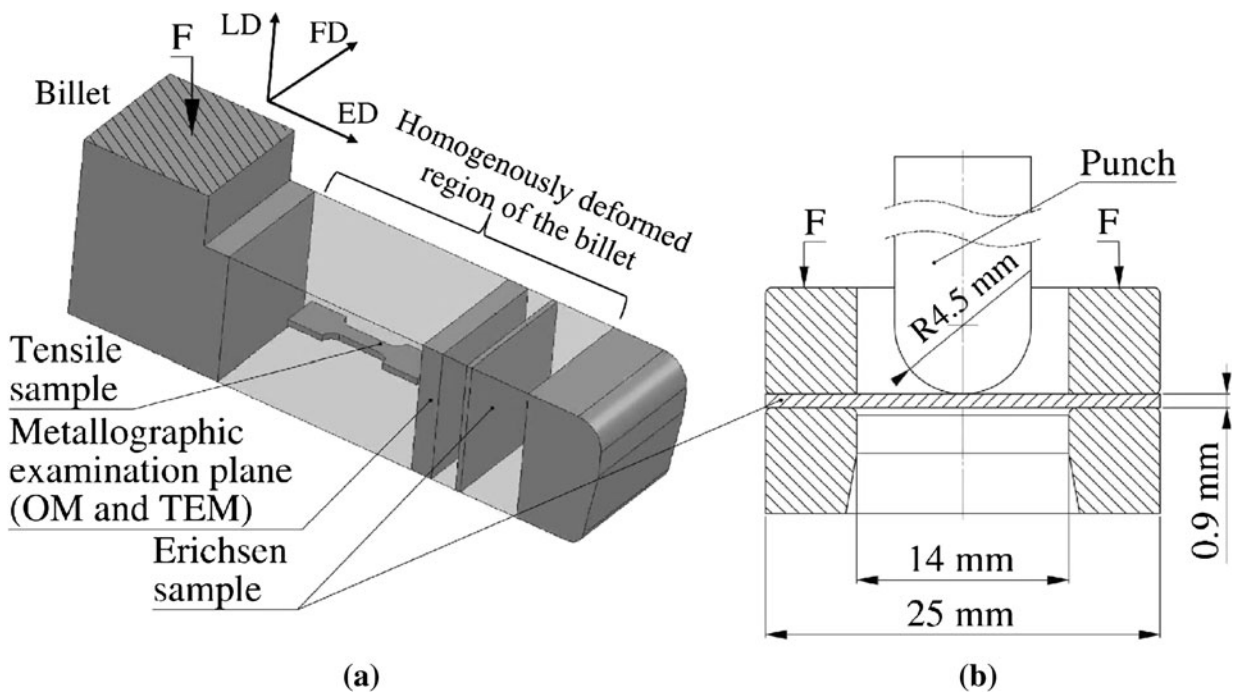

Fig. 1—Schematic illustrations showing (*a*) the position of the samples inside the ECAE-processed billet and (*b*) miniaturized Erichsen die.

25 V at 233 K (−40 °C). TEM was conducted using a Philips CM-200 microscope operated at a nominal voltage of 200 kV. Tensile properties were determined on dog bone-shaped samples with gage section of 1.2 mm × 3 mm × 8 mm using uniaxial tensile tests at a strain rate of $5.4 \times 10^{-4} \text{ s}^{-1}$. The tensile axis of the samples was oriented parallel to the extrusion direction as illustrated in Figure 1(a).

Stretch formability tests of CG and UFG IF-steel samples were performed using the Erichsen test technique, which is a well-established standard for studying the formability under biaxial strain conditions. The Erichsen test samples with the dimensions of 25 mm × 25 mm × 0.9 mm were sectioned from the transverse plane of the extruded billets using the wire-EDM technique (Figure 1(a)). The samples were machined from the uniformly strained region of the billets as shown in Figure 1(a). In practical applications, one criticism is that thin slices will unlikely be cut out from the ECAE billets for further processing as they were normal sheet metals. In this study, the aim was to see the sole effect of SPD-induced UFG microstructures on the formability under biaxial strain. If the bulk-processed billets were converted into sheet by upsetting or rolling, the resulting microstructure would change and a different formability response would result. Clearly, this further deformed microstructure would be more complex including the effects of both traditional processing of rolling or forging and ECAE processing (as pointed out in many published papers). Therefore, it is necessary to clearly separate the effects of the different processing steps on formability. Moreover, it should be possible to obtain a similar UFG microstructure in sheets using appropriate SPD techniques or modified equal-channel angular sheet extrusion. In this case, the forming behavior is expected to be the same as that observed in the present study.

The surfaces of the samples were ground using emery paper down to a grid size of 1000 and then polished with a 1-μm alumina solution before stretch tests. The tests were conducted using a miniaturized Erichsen die system attached to an Instron 3220 universal testing machine. The dimensions of this fixture were adjusted as 45 pct of the standard Erichsen test fixture according to ISO-EN 20482. A schematic illustration of this system is depicted in Figure 1(b). The tests were performed with a punch speed of 0.01 mm s^{-1} without lubrication, and the load–displacement data were collected during the tests. After the test, the Erichsen index (EI) and the load (F_{EI}) corresponding to this index were evaluated from the load–displacement curves. Morphological features of the stretched sample were examined using a JEOL JSM 6400 scanning electron microscope (SEM) operated in the secondary electron mode at 15 keV.

III. RESULTS

A. *Microstructure and Uniaxial Tensile Properties*

The microstructure of CG IF-steel consists of coarse and mostly equiaxed ferrite grains (Figure 2(a)). It is clearly seen in Figure 2 that multi-pass ECAE led to a substantial microstructural refinement and transformed the CG as-received microstructure to a UFG structure with some morphological and size differences based on the followed strain path (Figures 2(a) through (d)). After 8A ECAE processing, a microstructure mainly consisting of elongated cell blocks created by shear bands and sub-divided by mostly low-angle grain boundaries (LAGBs) was formed (Figure 2(b)).[35–37] The mean thickness and length of these blocks were around 300 and 900 nm, respectively, demonstrating that the resulting microstructure after 8A ECAE processing consisted of grains with a high aspect ratio. As can be seen in Figure 2(b), the length of some subgrain blocks reached 2 μm, while the block widths were more homogeneously distributed over the microstructure. The 8Bc ECAE processing brought about a more refined microstructure with an average grain size of 240 ± 30 nm. This microstructure mostly has equiaxed grain morphology due to the intersection of the shear planes during 90-deg rotation of the billet between repetitive passes (Figure 2(c)). The microstructure formed after 8C ECAE exhibited mostly equiaxed but coarser grains with 510 ± 12 nm grain size compared to that formed after 8Bc ECAE (Figure 2(d)). Given the experimental error, the grain sizes measured in the current study are nearly identical to those given in previous studies on UFG IF-steel. In all UFG microstructures, most of the dislocations are accumulated at the grain boundary regions, and the amount of dislocation decreases through the grain interiors.

Representative selected area diffraction (SAD) patterns obtained from the UFG microstructures are shown in the insets of the micrographs (Figures 2(b) through (d)). The SAD pattern of the 8Bc condition shows a significant spreading of spots that formed ring-type patterns. For the same imaging conditions, more spotty SAD patterns were observed in 8A- and 8C ECAE-processed samples. It is known that UFG microstructures obtained with ECAE processing are composed of a mixture of grains with high-angle grain boundaries (HAGBs) and LAGBs. The SAD pattern of a UFG microstructure that is dominated by HAGBs is expected to show a ring-type SAD pattern as seen in the 8Bc condition (Figure 2(c)).[38] By contrast, the spotty SAD patterns of the 8A and 8C conditions suggest the presence of a higher proportion of LAGBs in the microstructure as compared to the 8Bc condition. In fact, previous data from quantitative EBSD analysis of the microstructure present in UFG IF-steel correlate well with the findings of the current study. For instance, Gazder *et al.*[39] investigated the effect of processing route and number of passes on the microstructural refinement of the IF-steel using EBSD. They reported a mean grain size of about 0.5 μm and 44 pct of LAGBs after 8Bc ECAE processing. In that study, a comparison between the data obtained after processing *via* 4Bc and 4C was also made, and route-Bc was found to be the most effective route in grain refinement and transformation of the LAGBs into HAGBs. Niendorf *et al.*[24] also investigated the microstructure of 8C ECAE-processed IF-steel using EBSD data. They reported that
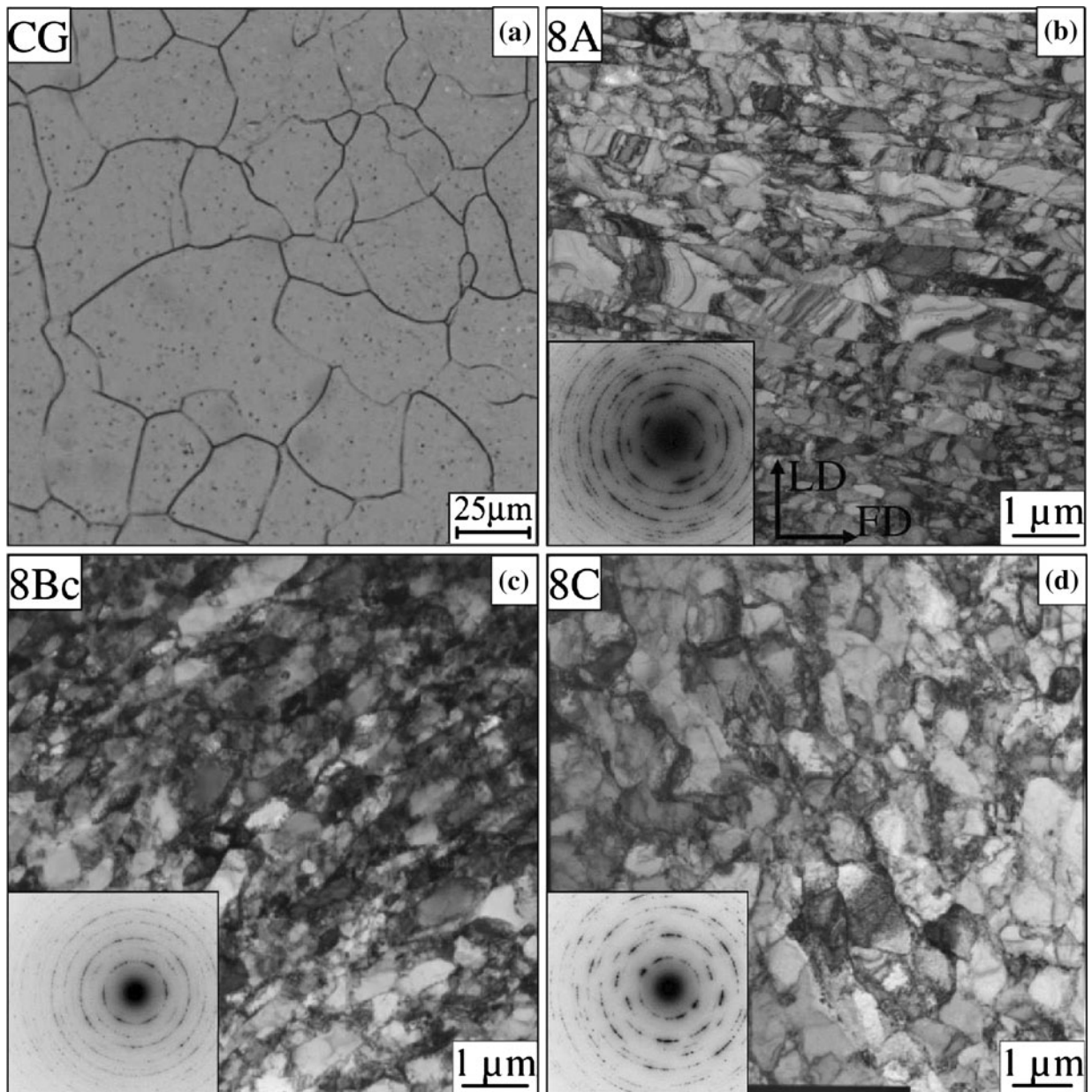
Fig. 2—(*a*) Optical microstructure of as-received CG IF-steel. TEM micrographs and SAD patterns showing the microstructure on the transverse planes of UFG IF-steel produced by ECAE following route (*b*) 8A, (*c*) 8Bc, and (*d*) 8C.

the microstructure was dominated by LAGBs inside larger grains that featured HAGBs. The volume fraction of the LAGBs after 8C-ECAE processing was around 60 pct in that study.

The stress–strain curves of the CG and UFG IF-steels are shown in Figure 3, and the corresponding mechanical properties are given in Table I. The CG IF-steel demonstrated limited strength, but high ductility. Formation of UFG microstructure increased the strength, but decreased the ductility of CG steel regardless of the routes. Such changes in these properties are very common in single-phase UFG metallic materials.[40,41] ECAE processing following 8A, 8Bc, and 8C increased the yield strength from 106 MPa to about 636, 687, and 568 MPa, respectively. Elongation to failure of UFG

IF-steel after processing by 8A, 8C, and 8Bc was determined as 9.6, 14.1, and 14.7 pct, respectively. Contrary to the as-received condition, UFG IF-steel demonstrated very limited uniform elongations in the range of 1.5 to 1.9 pct. This means that UFG considerably decreased the strain-hardening capacity of IF-steels and resulted in a relatively high post-uniform elongation (Figure 3). The substantial increase in the strength of UFG IF-steels can be attributed to the extensive grain refinement (Hall–Petch effect) and stored dislocations (dislocation hardening) formed during ECAE processing.[39,42] The decrease in the ductility after ECAE processing is attributed to the early onset of necking due to the limited strain-hardening capacity of the UFG microstructure.[4,40,41,43,44] Limited strain

hardening was reported especially for the single-phase UFG materials such as Cu,[40] Al,[41,44] and Ni.[45] Such behavior in UFG materials was explained in terms of limited dislocation interactions during the uniaxial tensile test.[40,41,43] The microstructure of UFG materials consists of refined grains surrounded by strain-induced dislocation boundaries. Therefore, the free path of dislocations is lower than that of CG microstructure.[41,43,44] Also, strain-induced grain boundaries act as dislocation traps which decrease the possible dislocation interactions through a short dislocation free path.

It can be seen in Table I that the tensile response somewhat depends on the applied strain path. For instance, the UFG microstructure formed after 8Bc has the finest grain size (Figure 2(c)) and thus produced the highest yield strength (Table I), whereas the largest grain size was obtained after 8C ECAE (Figure 2(d)) and therefore yielded the lowest yield strength (Table I). These results indicate that the Hall–Petch effect is qualitatively valid for these microstructures. Ductility of UFG IF-steel was slightly affected by the applied strain path. The material after 8A processing has the lowest elongation to failure. This may be due to the microstructure having strongly elongated grain morphology. In contrast, mostly equiaxed grain morphology was formed after 8Bc and 8C with very close elongation values to each other, but higher than those of the 8A-processed sample.
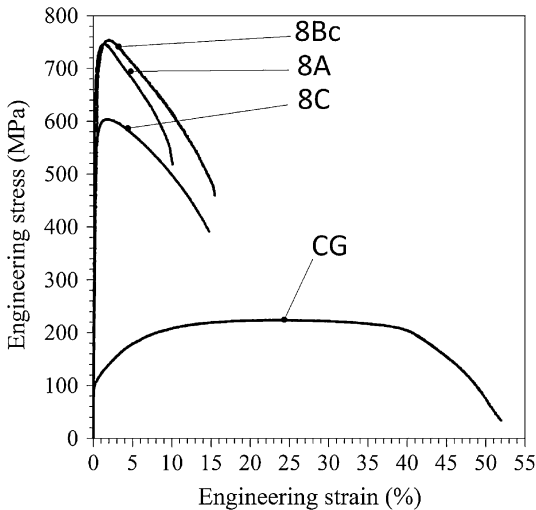
B. Biaxial Stretch Formability

1. Load–displacement curve

Load (F)–displacement (X) curves obtained from the Erichsen tests are presented in Figure 4(a). In addition, the values of the Erichsen index (EI) and punch load at EI (F_{EI}) determined from these curves are given in Table II. It is seen from F–X curves that deformation of CG and UFG samples takes place in several stages under biaxial stresses via the Erichsen tests as previously reported by Manahan et al.[46] In order to distinguish the deformation stages from each other, the first-order derivative of the punch load (F) with respect to the displacement (X) was calculated, and the dF/dX–X curves are depicted in Figure 4(b). In this figure, the load–displacement curve of the CG sample shows a
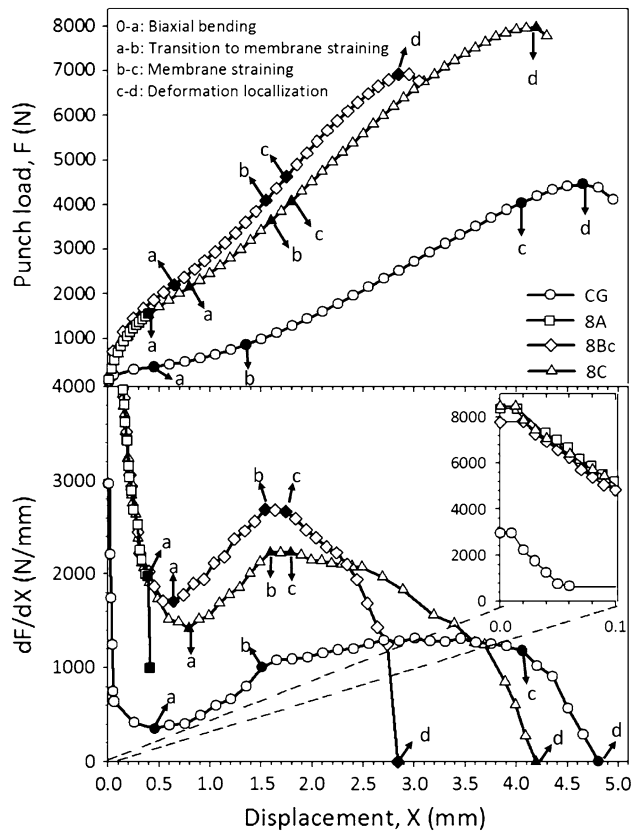
Fig. 4—(a) Punch load (F) vs displacement (X) curves obtained during Erichsen tests of CG and UFG IF-steel samples. (b) The dF/dX vs displacement (X) curves showing the stretch deformation stages under biaxial loading.

Fig. 3—Room temperature stress–strain curves of the CG and UFG IF-steel.

Table I. Uniaxial Tensile Properties of CG and UFG IF-Steels at Room Temperature

Condition	Yield Strength (MPa)	Tensile Strength (MPa)	Uniform Elongation (pct)	Elongation to Failure (pct)
CG	106 ± 02	232 ± 13	25.1 ± 2.2	53.0 ± 1.4
UFG				
8A	636 ± 15	724 ± 13	1.5 ± 0.2	9.6 ± 2.3
8Bc	687 ± 09	750 ± 06	1.8 ± 0.3	14.7 ± 1.5
8C	568 ± 08	601 ± 20	1.9 ± 0.2	14.1 ± 2.4

Table II. Erichsen Index (EI) with Corresponding Compressive Loads (F_{EI}) Before Fracturing the CG and UFG IF-Steel Samples

Condition	Erichsen Index (EI) (mm)	Load at Erichsen index (F_{EI}) (N)
CG	4.50 ± 0.20	4190 ± 400
UFG		
8A	0.35 ± 0.15	$1380 + 250$
8Bc	2.90 ± 0.30	6910 ± 200
8C	3.91 ± 0.20	7990 ± 140

narrow elastic deformation region, which is governed by both the Young's modulus and strength at the beginning of the punch travel as clearly shown in the inset of this figure.[46] Following elastic deformation, plastic deformation takes place by the formation of a yield zone at regions where the highest elastic displacement occurred. This is followed by the propagation of the yield zone along the cross section of the thickness and subsequently in radial directions.[46] This deformation stage is valid up to the point "a," the lowest dF/dX value in the first stage of the dF/dX vs X curve, as indicated in Figure 4(b). During propagation of the yield zone, the dF/dX decreases with increasing displacement (X), and plastic deformation mainly occurs through biaxial bending in this stage.[46] Further displacement of the punch transitions the deformation characteristic from biaxial bending into membrane straining between points "a" and "b" (Figure 4(b)).[46] In this stage, the dF/dX increases with increasing punch displacement up to point "b." After this point, the dF/dX–X curve becomes nearly steady state within the region between points "b" and "c" (Figure 4(b)). In this stage, the thickness of the plate decreased uniformly with the membrane straining as explained in Reference 46. A possible decrease in the punch load due to the decrease in the sheet thickness is balanced by the high strain-hardening capacity of CG IF-steel during stretching in the membrane-straining regime. This results almost in a steady state dF/dX–X curve (Figure 4(b)). Further deformation after point "c" caused deformation localization, and load–displacement curve reached the peak load at point "d".[46] Beyond this point, the punch load starts decreasing with crack initiation and propagation on the dome surface with further deformation. These letters indicating boundaries of the deformation stages in the Erichsen test and mark the changes in the slope of the curves.

Stretch formability of IF-steel under the biaxial loading condition was affected considerably by the formation of UFG microstructure depending on applied strain paths. The 8A ECAE-processed sample resulted in a limited biaxial stretch formability during the Erichsen test and fractured just after a small punch displacement (Figure 4(a)). As can be seen in Figure 4(b), the fracture occurred during the biaxial bending stage without considerable stretch deformation. On the other hand, the 8C- and 8Bc-processed samples demonstrated higher stretch formability during the Erichsen tests compared to the 8A sample (Figure 4(b)). Also, the deformation behavior of 8C- and 8Bc-pro-

cessed samples under biaxial loading is identical to that of the CG sample up to the membrane-straining region (point "b"). However, contrary to the CG sample, the steady state region between points "b" and "c" is very narrow in the UFG samples. The dF/dX decreased continuously with punch displacement after point "c" in the membrane-straining regime.

As seen in Table II, CG IF-steel exhibited the highest formability with the EI value of 4.50 mm. The EI values of 8A-, 8Bc-, and 8C-processed samples were found to be 0.35, 2.90, and 3.91 mm, respectively. It is also obvious from these values that the highest and lowest formability was obtained from 8C- to 8A-processed samples, respectively. On the other hand, the high strength of the UFG samples increased the required load (punch load) for plastic deformation during the Erichsen test, except the sample processed by route 8A. From Table II, the F_{Ei} was determined as 4190 N for the CG condition. This value increased to about 7990 and 6910 N after processing by routes 8C and 8Bc, respectively. However, the F_{EI} of the sample processed by route 8A was determined as 1380 N, which is much lower than those of CG and other UFG IF-steels.

2. Surface and sub-surface features after biaxial stretching

SEM micrographs representing the free dome surfaces of the CG and UFG samples after the Erichsen tests are shown in Figures 5 through 8. Figures 5(a) and (b) shows that the smoothness of the initially polished surface of the CG sample was transformed into the rough free surface with the formation of the orange peel effect after stretching via the Erichsen test.[47] Roughening of the free surface with an orange peel effect is shown in Figure 5(c) at a higher magnification. Also, shallow tears formed on the grain surfaces as can be seen in Figure 5(d). These tears have a misorientation to those formed in the neighboring grain. This may be taken as an indicator of variation of the plastic deformation behavior in adjacent grains. The surface morphology and fracture characteristics of CG microstructure are substantially changed by intense deformation via ECAE depending on the applied strain path. Surface appearances of the stretched 8A-processed sample are represented in Figure 6. It can be clearly seen that this sample did not deform into a dome shape due to the early onset of fracture with an EI value of 0.35 mm (Figure 6(a)). During stretching, cracks suddenly formed at the central part of the sample, where semi-spherical punch first contacted the sample, and propagated through the inclination angle of the prior grain boundaries after ECAE and following the cell-block boundaries (Figure 6(a)). Figure 6(b) shows the strain localization regions at the tip of the crack, where many micro-cracks propagated parallel to each other almost along the flow direction (FD)(defined in Figure 1), helping the formation of the main crack path. This direction is nearly coincident with the elongated grain boundaries seen in Figure 2(b).

The surface appearances of the biaxial stretched 8C- and 8Bc-processed samples are presented in Figures 7
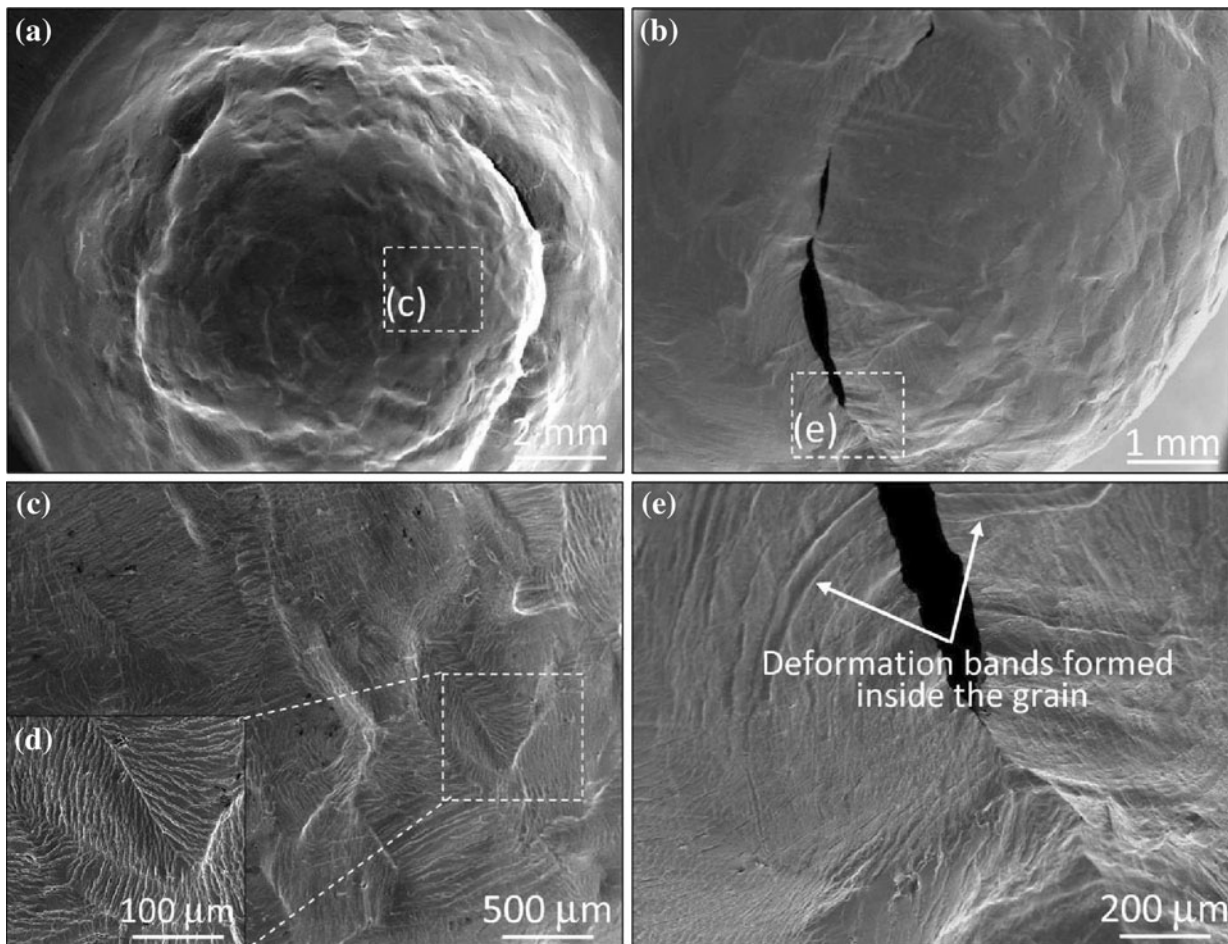
Fig. 5—SEM micrographs showing the roughening of the dome free surface of Erichsen-tested CG IF-steel sample: (*a*) General dome view showing orange peel effect, (*b*) side view of the dome surface with fracture, (*c*) high magnification image of orange peel formation, (*d*) misoriented deformation of neighboring grains leading to orange peel effect, and (*e*) fracture propagation region with deformation bands on the dome surface.
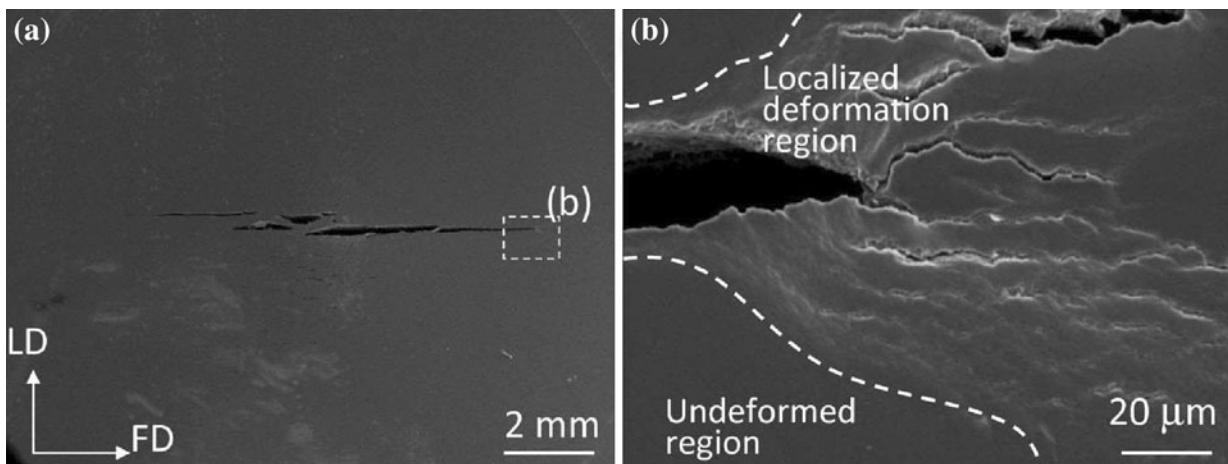

Fig. 6—SEM micrographs showing the biaxial stretched surface of the 8A-processed UFG sample: (*a*) General view of stretched sample showing the cracks and (*b*) high magnification micrograph showing the crack propagation and deformation localization region.

and 8. The samples strained considerably under biaxial loading and deformed into the dome shape as in the case of the CG one. It is also evident from the SEM micrographs (Figures 7 and 8) that there is a substantial

reduction in mesoscale roughening (called orange peel effect) on the dome surface of the UFG samples processed by routes 8Bc and 8C. From the SEM micrographs, it is also possible to say that stretching
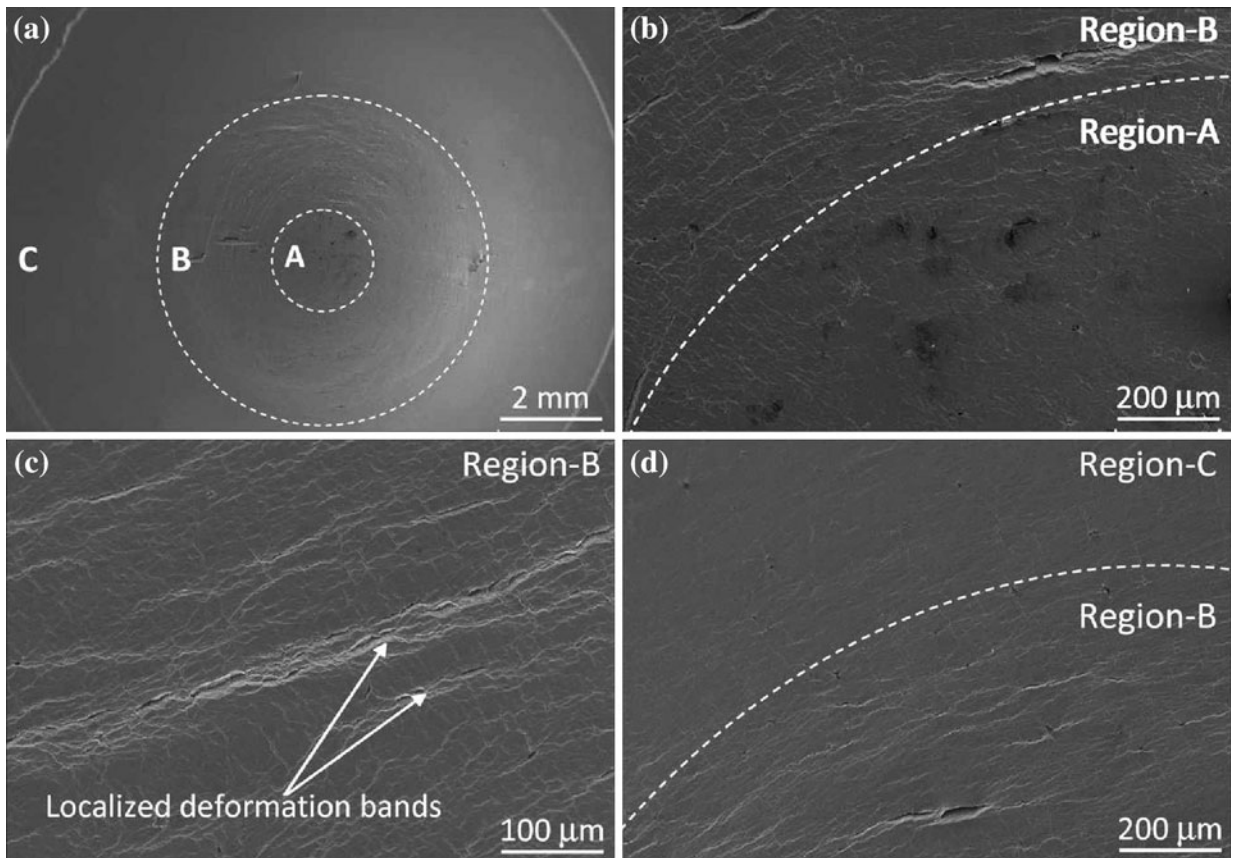
Fig. 7—SEM micrographs showing the morphological features of the dome surface of the biaxial stretched sample previously processed by ECAE 8Bc: (*a*) A general view showing different deformation regions, namely region-A formed under the effect of frictional forces, region-B stretched with biaxial tensile loads, and region-C deformed with biaxial bending. (*b*) A detailed view of region-A and the boundary between region-A and region-B. (*c*) A detailed view of region-B showing the deformation bands. (*d*) Smooth surface appearance of region-C indicating that no considerable amount of deformation occurs during stretching.

under biaxial tensile loading caused the formation of three main deformation regions in these samples, called region-A, region-B, and region-C, each of which has different surface appearances with different deformation homogeneity. The surface morphologies obtained in each region are identical for both routes as indicated on the SEM micrographs (Figures 7 and 8). SEM micrographs taken from region-A of the 8C- and 8Bc-processed samples are shown in Figures 7(b) and 8(b), respectively. These micrographs show that limited numbers of shallow cracks and/or tearing form at the surface of the region-A (central region of the dome surface). In this region, the friction force in-between the punch and sample surface during stretching may counteract the stretching effect. Therefore, even if the central region of the sample has the highest deflection, only shallow surface cracks and/or tears form at that region. Also, Figures 7(b) and 8(b) represent the transition of the smooth dome free surface at region-A to the rougher surface appearance that can be characterized with localized deformation bands formed at region-B. High magnification micrographs showing the deformation bands with micro-cracks formed at region-B are shown in Figures 7(c) and 8(c). A smooth surface just as in the case of the initially polished state is seen in region-C (Figures 7(d) and 8(d)). This indicates that region-C of

the 8C- and 8Bc-processed samples does not undergo considerable plastic deformation with membrane straining, but was deformed within the biaxial bending regime during the Erichsen test. This may be because of the early deformation localization formed in region-B during stretching (Figures 7(c) and 8(c)).

The dome surface regions can also be validated with the variations in the thickness of biaxial stretched samples. Therefore, the cross sections of the domes with the corresponding thickness values are shown in Figure 9. It is obvious from Figure 9 that the initial thickness (0.9 mm) of the CG, 8Bc, and 8C samples was decreased to 0.70, 0.85, and 0.80 mm, respectively at the region under the effect of punch friction (region-A). Hence, it can be concluded that both CG and UFG samples were not thinned considerably during biaxial stretching at that region, which also led to smoother surfaces than that at region-B (Figures 7(a) and 8(a)). This is probably because of the significant friction at the punch-sample interface and thus lower amount of thinning. At the localized deformation region (region-B), the thickness of the samples decreased considerably with necking and finally fracture occurred (Figure 9). This may be due to the coalescence of dislocations, which results in micro-voids as a typical reason for plastic instability with necking of CG samples after large plastic deformations.[30] The
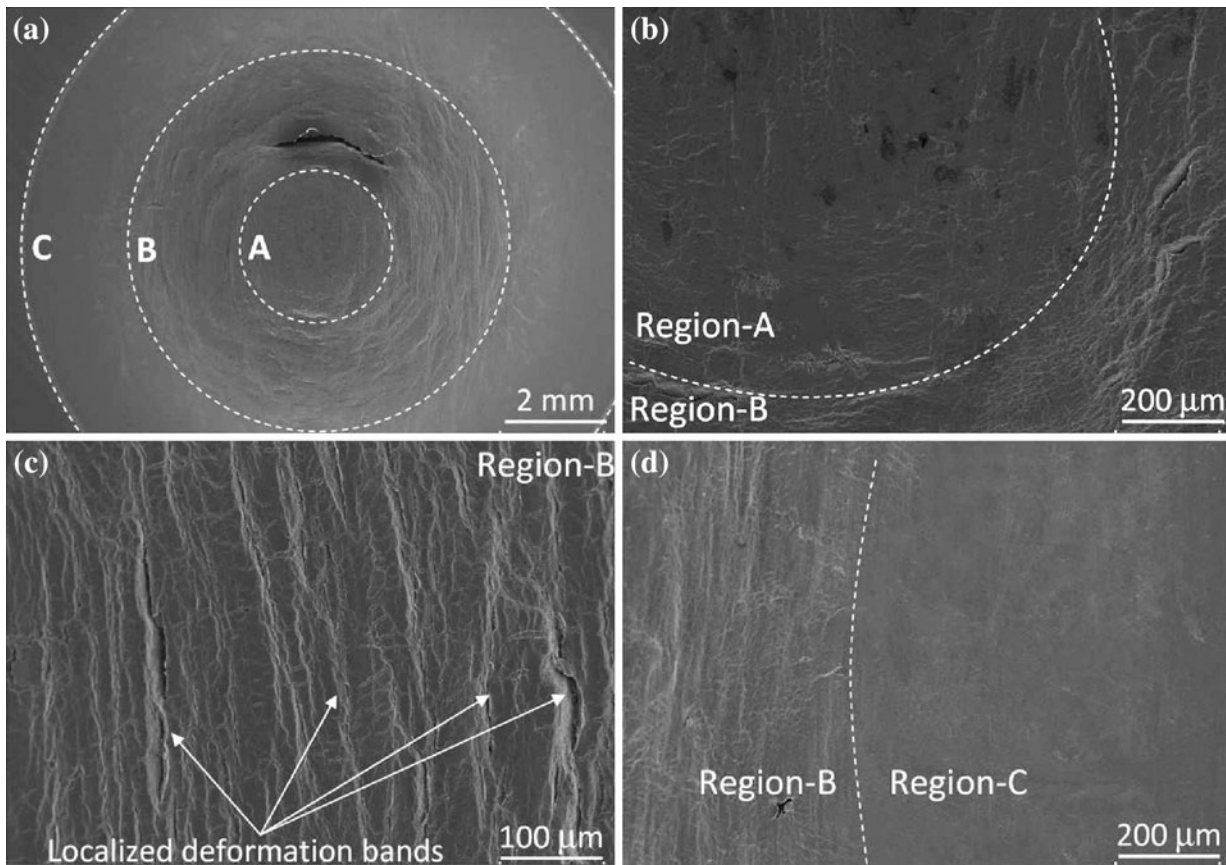
Fig. 8—SEM micrographs showing the morphological features of the dome surface of the Erichsen-tested sample previously processed by ECAE 8C: (*a*) A general view showing different deformation regions, namely region-A under the effect of frictional forces, region-B stretched with biaxial tensile loads, and region-C deformed with biaxial bending. (*b*) A detailed view of region-A and the boundary between region-A and region-B. (*c*) A detailed view of region-B showing the deformation bands. (*d*) Smooth surface appearance of region-C indicating that no considerable amount of deformation occurs during deformation.

thickness of the CG samples at that region is much lower than those of UFG samples. It was about 0.45 mm, which means a considerable amount of deformation (uniform thinning) took place before necking during stretch forming of the CG sample. Localized deformation regions (region-B) observed at dome free surfaces of the 8Bc- and 8C-samples (Figures 7(c) and 8(c)) also show local thinning of the sample, but not as much as that in the case of the CG sample. Average thicknesses of the localized deformation regions were determined as 0.70 and 0.51 mm for the 8Bc- and 8C-processed samples, respectively. This is because of the limited uniform deformation capacity of the ECAE-processed samples during secondary deformation of stretching as in the case of uniaxial tensile deformation (Table I). In the bended region (region-C), the samples are not thinned considerably. Dome thicknesses at region-C were determined as 0.90 mm for the 8Bc-processed and 0.88 mm for the 8C-processed samples, which are very close to the initial thickness (0.9 mm) of the samples. This may be because of the limited plastic deformation in that region during stretching. After strain localization, most of the deformation takes place in the localized region (region-B), and thus the thickness in the bended region remains nearly constant especially for the UFG samples.

IV. DISCUSSION

The grain refinement *via* ECAE strongly affected the formability and surface quality of the IF-steel samples depending on the applied strain path. The ECAE processing using route 8A resulted in a limited biaxial stretch formability, and the sample fractured just after a slight punch displacement without considerable deformation (Figure 4(a)). This limited formability can be explained in terms of the strongly elongated UFG microstructure formed after the 8A processing. The TEM micrograph (Figure 2(b)) and the dome free surface appearance after stretching (Figure 6) confirm that the cracks initiate and propagate through the boundaries of cell blocks. This means that elongated grain boundaries act as easy crack initiation and propagation regions, where high stress concentrations leading to high cracking tendency were accumulated during initial ECAE processing. Therefore, these boundaries are becoming easy paths for the crack propagation especially under biaxial loading conditions. This resulted in lower F_{EI} and EI values compared to other routes, even though comparable strength values were obtained under uniaxial tensile test. Niendorf *et al.*[30] also discussed the effect of microstructural features on
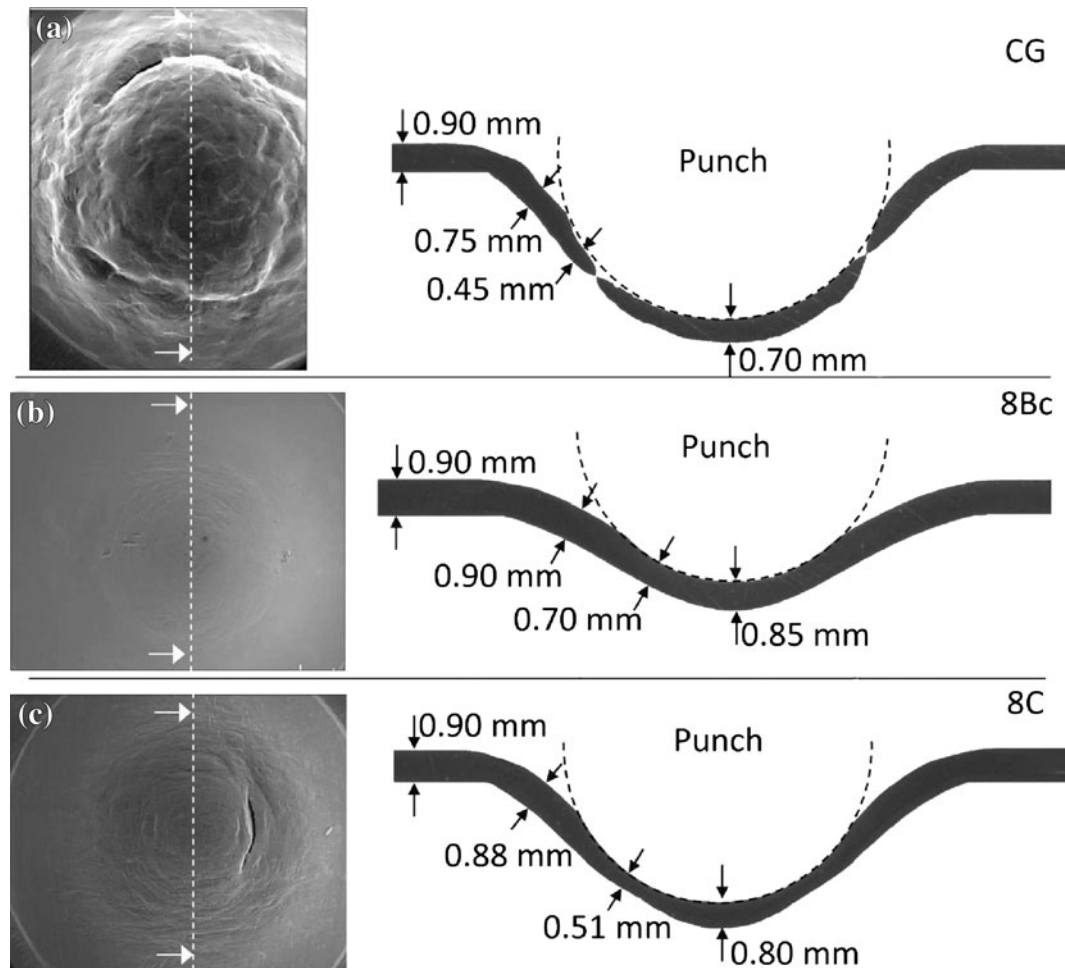
Fig. 9—Variation in the thickness of the CG and UFG samples after biaxial stretching *via* the Erichsen test.

the crack propagation behavior of the UFG IF-steels during fatigue testing. They concluded that the microstructural features such as elongated grain/subgrain boundaries causing stress concentrations may act as the places where crack propagation occurs easily under cyclic loading conditions. Similarly, such microstructural features obtained in this study by route-A seem to have a considerable effect on the cracking tendency and overall mechanical performance under biaxial loading conditions. A higher cracking tendency due to the elongated boundaries was also observed in the uniaxial tension tests and can be understood based on the lower tension ductility of the 8A IF-steel in uniaxial tensile tests compared to 8C and 8Bc (Figure 3). This influence becomes more pronounced under biaxial loading conditions due to the multiaxial tension stress condition, which may initiate cracks more easily in the case of the Erichsen testing of the 8A IF-steel.

The UFG microstructures that formed after the 8Bc and 8C processing showed relatively high formability under biaxial loading in contrast to those formed after the 8A processing, which can be attributed to the microstructural differences. The ECAE processing following route-Bc and route-C results in a microstructure mainly consisting of equiaxed ultrafine grains (Figures 2(c) and (d)). This grain morphology results in lower cracking tendency and higher EI and F_{EI} values after stretching compared to those of the 8A-processed condition (Table II). However, such a UFG microstructure still yields F–X curves with a decreasing slope just after the transition to the membrane-straining regime in contrast to the CG microstructure (Figure 4(b)). This is due to the limited strain-hardening capacity of the 8C- and 8Bc-processed UFG samples as shown in Figure 3. According to the results obtained from the uniaxial tensile tests, uniform elongation of the CG IF-steel was decreased from 25 pct to about 2 pct after ECAE processing following routes 8C and 8Bc. This means that very limited strain hardening may also occur during secondary deformation processes like deep drawing. Therefore, the 8C- and 8Bc-processed samples cannot compensate the decrease in the punch load due to the thinning of the sample by strain hardening in the membrane-straining regime. This causes early localization of the deformation as in the case of the biaxial tensile test and consequently, the dF/dX curve continues to decrease with the punch displacement up to the point "d," the peak point of the load–displacement curve as shown in Figure 4(b). This indicates that not only

uniaxial tensile elongation but also biaxial deformation of the UFG IF-steel takes place mostly in a heterogeneous manner due to the limited strain-hardening capacity, and a great proportion of the tensile elongation occurs *via* plastic instability with the formation of localized deformation bands (Table II).[24,40,44]

The microstructural differences in the samples obtained by the 8Bc and 8C conditions brought about a minor deviation in the formability behavior. The microstructure of the 8Bc-processed sample consists of finer and well-defined grains compared to that of the 8C-processed sample (Figure 2(c)). Hence, dislocations stored in that microstructure are mostly accumulated at or near the grain boundaries. Contrary to the 8Bc condition, dislocations are accumulated not only at grain boundaries but also in grain interiors of the coarser grains in the microstructure of the 8C-processed sample (Figure 2(d)). Furthermore, the 8Bc processing forms a higher fraction of HAGBs as compared to route-C as discussed previously.[39] The higher amount of HAGBs in the microstructure means a higher amount of internal energy (Figure 2(c)). Such a microstructure with the higher energy state of the grain boundaries may cause an increase in the cracking tendency under biaxial tensile loading and therefore cause lower EI and F_{EI} values compared to those of the 8C-processed sample.[50]

It should be noted that it is not possible to establish a direct correlation between the strength and ductility values obtained in uniaxial tensile tests and the EI and F_{EI} values obtained in biaxial Erichsen tests. The highest and the lowest strength levels were obtained from the samples processed with ECAE 8Bc and 8C, respectively (Table I). Also, the strength of the 8A-processed sample was close to that of the 8Bc-processed sample. The uniaxial tensile ductility by means of uniform elongation and elongation to failure of the 8Bc- and 8C-processed samples was very close to each other and somehow higher than those of the 8A-processed sample. Even though the lowest strength was obtained in the 8C-processed sample using the uniaxial tensile test, its F_{EI} value was the highest in the case of biaxial deformation. In addition, the highest EI value was measured in the 8C-processed sample, though the 8Bc-processed sample has similar elongation values. Moreover, the 8A-processed sample shows the lowest EI and F_{EI} even though the uniaxial tensile properties are comparable to those of the 8C- and 8Bc-processed samples. Therefore, it can be stated that it is not possible to find a direct correlation between the results from the uniaxial tensile tests and biaxial Erichsen test.

Surface appearance is important after the forming of sheet metals, considering their applications. The SEM micrographs (Figures 7 and 8) clearly showed that the surface quality improved with fine grain formation. The orange peel effect (grainy surface) generally occurs in CG materials due to the deformation incompatibilities in the neighboring grains as a result of difference in the crystallographic orientation of the grains.[47,48] Such deformation incompatibilities are clearly seen in Figure 5(c) and (d), where micro-shear bands with different orientations formed at the free surface of each coarse grain oriented in different directions compared to

the adjacent ones. Consequently, the grains stand out in relief on the surface. Surface roughening of the CG sample can be seen throughout the free surface of the sample in Figure 5(b). This figure also represents the failure mode of the sample, which is circumferentially caused by cracks that propagated through the grain interiors. This may indicate that crack initiation took place as a result of micro-void formation (Figure 5(e)). In contrast to the CG samples, the formation of a UFG microstructure reduced the orange peel effect and roughening on the dome surface of the UFG samples considerably. This positive effect was most pronounced after processing along routes 8Bc and 8C. The individual grains in the UFG microstructure are too small to detect the surface relief which reflected improved surface quality.

These results showed that the UFG microstructure decreased the formability of CG microstructure depending on the applied strain paths. This may be the problem of using UFG materials for further processing to obtain final products or semi-products. However, the results also indicate that the formability of UFG microstructures having mostly equiaxed grains can be improved further by secondary processing before shaping. For instance, appropriate heat treatment should allow for an optimization between strength and ductility or formability.

V. CONCLUSIONS

In this study, the effects of UFG microstructures produced following different ECAE routes on the biaxial stretch formability of IF-steels were investigated. The main results and conclusions of this study can be summarized as follows:

1. Ultrafine-grained microstructures having grain sizes in the range of 240 to 510 nm were obtained from the coarse-grained (*d*: ≈30 μm) IF-steel with ECAE following different strain paths. Such grain refinement along with high density of dislocations leads to a significant increase in the tensile strength values in the expense of ductility under uniaxial loading condition, regardless of the processing routes.

2. The CG samples demonstrated high formability and deformed uniformly under biaxial loading conditions due to its high strain-hardening capacity. The grain refinement by multi-pass ECAE processing has a strong effect on the formability of IF-steel depending on the applied strain paths that lead to different grain sizes and grain morphology. Heavily elongated microstructure formed after the 8A processing caused early fracture of the sample and yielded the lowest EI and F_{EI} values due to the high cracking tendency as a result of the stress concentrations at the elongated grain boundaries. Contrary to the 8A-processed sample, the samples previously processed by routes 8C and 8Bc could be considerably deformed under biaxial loading and into the dome shape as in the case of the CG one due to the equiaxed grain morphology having relatively

low cracking tendency. Also, a much higher punch force was needed for stretching high strength UFG IF-steels compared to those for the CG one.

3. The stretching under biaxial tensile loading caused the formation of three main deformation regions in the 8Bc- and 8C-processed UFG samples. In region-A, no considerable thinning and cracks were observed due to the frictional force in-between the punch and sample surface on the central region of the dome surface. In region-B, many localized deformation bands with micro-cracks occurred during stretching. No considerable amount of deformation took place in region-C.

4. It is not possible to establish a direct correlation between the strength and ductility values obtained in uniaxial tensile test and the EI and F_{EI} values obtained in the biaxial Erichsen test.

5. The surface quality of the stretched samples was improved by grain refinement *via* ECAE, and non-uniform grain flow leading to the so-called orange peel effect on the dome free surface of the CG sample was considerably reduced after UFG formation.

6. The UFG microstructures can be substantially deformed even under the biaxial stretching process if a microstructure with mostly equiaxed grain morphology can be obtained using ECAE following suitable strain paths, even though the same microstructures can lead to very low ductility under uniaxial loading conditions.

REFERENCES

1. U. Engel and R. Eckstein: *J. Mater. Process. Technol.*, 2002, vols. 125–126, pp. 35–44.
2. U. Engel, A. Rosochowski, S. Geißdörfer, and L. Olejnik: *Microforming and Nanomaterials*, Springer, Paris, 2007, pp. 99–124.
3. V.M. Segal: *Mater. Sci. Eng. A*, 2004, vol. 386, pp. 269–76.
4. R.Z. Valiev and T.G. Langdon: *Prog. Mater Sci.*, 2006, vol. 51, pp. 881–981.
5. Y.T. Zhu, T.C. Lowe, and T.G. Langdon: *Scripta Mater.*, 2004, vol. 51, pp. 825–30.
6. G.G. Yapici, C.N. Tome, I.J. Beyerlein, I. Karaman, S.C. Vogel, and C. Liu: *Acta Mater.*, 2009, vol. 57, pp. 4855–65.
7. G.G. Yapici, I. Karaman, and H.J. Maier: *Mater. Sci. Eng. A*, 2006, vol. 434, pp. 294–302.
8. G.G. Yapici, I.J. Beyerlein, I. Karaman, and C.N. Tome: *Acta Mater.*, 2007, vol. 55, pp. 4603–13.
9. G. Purcek, G.G. Yapici, I. Karaman, and H.J. Maier: *Mater. Sci. Eng. A*, 2011, vol. 528, pp. 2303–08.
10. G. Purcek, O. Saray, O. Kul, I. Karaman, G.G. Yapici, M. Haouaoui, and H.J. Maier: *Mater. Sci. Eng. A*, 2009, vol. 517, pp. 97–104.
11. G. Purcek, O. Saray, I. Karaman, and M. Haouaoui: *Metall. Mater. Trans. A*, 2009, vol. 40A, pp. 2772–83.
12. H.J. Maier, P. Gabor, and I. Karaman: *Mater. Sci. Eng. A*, 2005, vol. 410, pp. 457–61.
13. I. Karaman, M. Haouaoui, and H.J. Maier: *J. Mater. Sci.*, 2007, vol. 42, pp. 1561–76.
14. H.S. Kim, M.H. Seo, and S.I. Hong: *J. Mater. Process. Technol.*, 2001, vol. 113, pp. 622–26.
15. M. Furukawa, Y. Iwahashi, Z. Horita, M. Nemoto, and T.G. Langdon: *Mater. Sci. Eng. A*, 1998, vol. 257, pp. 328–32.
16. A. Rosochowski, W. Presz, L. Olejnik, and M. Richert: *Int. J. Adv. Manuf. Technol.*, 2007, vol. 33, pp. 137–46.
17. W. Presz and A. Rosochowski: *9th Int. Conf. Mater. Form. ESAFORM 2006*, A. Rosochowski and N.P. Juster, eds., Glasgow, United Kingdom, 2006, pp. 587–90.
18. X. Ma, R. Lapovok, C. Gu, A. Molotnikov, Y. Estrin, E. Pereloma, C. Davies, and P. Hodgson: *J. Mater. Sci.*, 2009, vol. 44, pp. 3807–12.
19. S. Hoile: *Mater. Sci. Technol.*, 2000, vol. 16, pp. 1079–93.
20. K. Banerjee, A. Verma, and T. Venugopalan: *Metall. Mater. Trans. A*, 2008, vol. 39A, pp. 1410–25.
21. W. Jeong: *Metall. Mater. Trans. A*, 2000, vol. 31A, pp. 1305–07.
22. O. Saray, G. Purcek, I. Karaman, T. Neindorf, and H.J. Maier: *Mater. Sci. Eng. A*, 2011, vol. 528, pp. 6573–83.
23. T. Niendorf, H.J. Maier, D. Canadinc, and I. Karaman: *Mater. Sci. Eng. A*, 2009, vol. 503, pp. 160–62.
24. T. Niendorf, D. Canadinc, H.J. Maier, and I. Karaman: *Int. J. Fatigue*, 2008, vol. 30, pp. 426–36.
25. T. Niendorf, D. Canadinc, H.J. Maier, and I. Karaman: *Metall. Mater. Trans. A*, 2007, vol. 38A, pp. 1946–55.
26. T. Niendorf, D. Canadinc, H.J. Maier, I. Karaman, and S.G. Sutter: *Int. J. Mater. Res.*, 2006, vol. 97, pp. 1328–36.
27. J. De Messemaeker, B. Verlinden, and J. Van Humbeeck: *Mater. Lett.*, 2004, vol. 58, pp. 3782–86.
28. B. Han, F. Mohamed, and E. Lavernia: *Metall. Mater. Trans. A*, 2003, vol. 34A, pp. 71–83.
29. H.S. Kim, W.S. Ryu, M. Janecek, S.C. Baik, and Y. Estrin: *Adv. Eng. Mater.*, 2005, vol. 7, pp. 43–46.
30. T. Niendorf, F. Rubitschek, H. Maier, D. Canadinc, and I. Karaman: *J. Mater. Sci.*, 2010, vol. 45, pp. 4813–21.
31. G. Purcek, O. Saray, I. Karaman, and T. Kucukomeroglu: *Mater. Sci. Eng. A*, 2008, vol. 490, pp. 403–10.
32. G. Purcek, O. Saray, I. Karaman, and H.J. Maier: *Metall. Mater. Trans. A*, 2012, vol. 43A, pp. 1884–94.
33. R. Yoda, K. Shibata, T. Morimitsu, D. Terada, and N. Tsuji: *Scripta Mater.*, 2011, vol. 65, pp. 175–78.
34. A. Sivaraman and U. Chakkingal: *J. Mater. Process. Technol.*, 2008, vol. 202, pp. 543–48.
35. N. Hansen, X. Huang, and D.A. Hughes: *Mater. Sci. Eng. A*, 2001, vol. 317, pp. 3–11.
36. D.A. Hughes, Q. Liu, D.C. Chrzan, and N. Hansen: *Acta Mater.*, 1997, vol. 45, pp. 105–12.
37. P.C. Wu, C.P. Chang, and P.W. Kao: *Mater. Sci. Eng. A*, 2004, vol. 374, pp. 196–203.
38. V.V. Stolyarov, Y.T. Zhu, I.V. Alexandrov, T.C. Lowe, and R.Z. Valiev: *Mater. Sci. Eng. A*, 2001, vol. 299, pp. 59–67.
39. A.A. Gazder, W. Cao, C.H.J. Davies, and E.V. Pereloma: *Mater. Sci. Eng. A*, 2008, vol. 497, pp. 341–52.
40. Y.M. Wang and E. Ma: *Acta Mater.*, 2004, vol. 52, pp. 1699–1709.
41. C.Y. Yu, P.W. Kao, and C.P. Chang: *Acta Mater.*, 2005, vol. 53, pp. 4019–28.
42. D.A. Hughes and N. Hansen: *Acta Mater.*, 2000, vol. 48, pp. 2985–3004.
43. D. Shin: *Met. Mater. Int.*, 2001, vol. 7, pp. 573–77.

44. C.Y. Yu, P.L. Sun, P.W. Kao, and C.P. Chang: *Scripta Mater.*, 2005, vol. 52, pp. 359–63.
45. N. Krasilnikov, W. Lojkowski, Z. Pakiela, and R. Valiev: *Mater. Sci. Eng. A*, 2005, vol. 397, pp. 330–37.
46. M.P. Manahan, A.E. Browning, A.E. Argon, and O.K. Harling: *Miniaturized Disc Bend Test Technique Development and Application, The Use of Small-Scale Specimens for Testing Irradiated Material*, ASTM, Albuquerque, NM, 1986.
47. R. Becker: *Acta Mater.*, 1998, vol. 46, pp. 1385–401.
48. O. Wouters, W.P. Vellinga, R.V. Tijum, and J.T.M. de Hosson: *Acta Mater.*, 2005, vol. 53, pp. 4043–50.